Objective assessment of nanoparticle disposition in mammalian skin after topical exposure

Christopher S. J. Campbell[*], L. Rodrigo Contreras-Rojas,
M. Begoña Delgado-Charro, and Richard H. Guy[$]

University of Bath
Department of Pharmacy & Pharmacology
Claverton Down
Bath, BA2 7AY, UK
[$]Correspondence: r.h.guy@bath.ac.uk; tel. +44.1225.384901; fax +44.1225.386114

*Present address: Mango Business Solutions, 2 Methuen Park, Chippenham, SN14 0GB, UK

Keywords: nanoparticles; skin; dermal exposure; laser scanning confocal microscopy; sebum

TOC GRAPHIC

Disposition of fluorescent nanoparticles on skin surface close to a hair emerging from its follicle. Particles are green, skin autofluorescence is red, sebum coating hair shaft is blue.

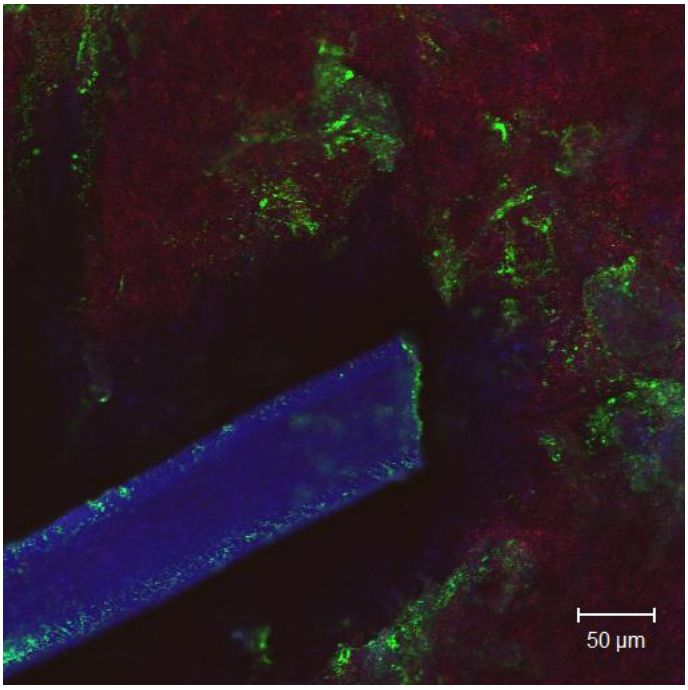

ABSTRACT

The use of nanoparticles as formulation components of topical drug delivery systems for the skin has been widely investigated in the literature. Because of the conflicting conclusions resulting from these studies concerning the ultimate disposition of the nanoparticles employed, the research presented in this paper has been designed to evaluate objectively the fate of such structures when administered to mammalian skin. Confocal microscopy images of skin exposed to nanoparticles have therefore been assessed by quantitative statistical analysis. Sebum on the skin surface was naturally fluorescent and clearly defined the outermost part of the cutaneous barrier. Fluorescent polystyrene nanoparticles applied in aqueous suspension could infiltrate only the stratum disjunctum, i.e., skin layers in the final stages of desquamation. This minimal uptake was independent of contact time (up to 16 hours) and of nanoparticle size tested (20-200 nm). When skin barrier function was modestly compromised, the nanoparticles remained incapable of penetration beyond the most superficial layers, corresponding to a depth of 2-3 μm, of the stratum corneum (the outermost, 15-20 μm skin layer). Overall, these results demonstrate objectively and semi-quantitatively that nanoparticles contacting intact, and even partially damaged, skin cannot penetrate beyond the superficial layers of the barrier, and are highly unlikely, therefore, to reach the viable cells of the epidermis or beyond. It follows that nanoparticulate-based, topical delivery systems may prove useful as skin surface reservoirs from which controlled drug release over time may be achieved.

INTRODUCTION

Nanotechnology is rapidly becoming integrated into many areas of manufacturing. Exposure to nano-scale objects either intentionally (through the use of cosmetics, for example, or via administration of topical, oral and injected medicines) or accidentally in the workplace (e.g., contact with coatings, dyes, composite materials, etc.) is therefore increasing. As a result, there is concern that these nanomaterials pose a greater health risk because their properties differ from those of the bulk substances [1]. For example a widely used "inert" compound, carbon black, in nanoparticulate form, appears to induce inflammatory signalling in lung cell cultures by generating reactive oxygen species [2]. Silica nanoparticles (<50 nm), on the other hand, do not have this effect but have been shown to damage keratinocytes whereas larger particles do not [3]. Since the toxicity of a material depends upon how easily it reaches the site of action, a detailed understanding of whether, and to what extent, nanoparticles are able to enter the body is vitally important. Equally, the opportunities presented by “nanomedicine” have led to a very broad examination of the potential of nanoparticles as drug delivery vectors, including their use in topical formulations designed to treat skin disease, or to facilitate systemic access via the transdermal route [4,5]. Despite the obvious challenge presented by the skin to the ingress of even very small particulate materials, the debate continues as to how such nano-structures can improve cutaneous, or even systemic, bioavailability of associated drugs.

The skin represents a major barrier to many environmental, chemical and biological assaults [6]. The outermost layer of the skin is the stratum corneum, a water-resistant “wall” of terminally-differentiated keratinocytes (called corneocytes) “riveted” together via corneodesmosomes [7] and damp-proofed by a “mortar” consisting of highly organized lipid lamellae. The skin is an excellent barrier to micro-organisms, macromolecules, and significantly retards the outward transport of water and the inward diffusion of small molecules. However, the evidence whether nanoparticles can infiltrate into underlying tissues is conflicting [4,5], and clarification of the issue is essential, not only for individuals with normal barrier function but also, more importantly, for those with compromised skin due to disease (e.g., eczema) or physical abrasion.

Investigations employing transmission electron microscopy [8,9] and atomic spectroscopy [10,11] have suggested that inorganic zinc oxide and titanium dioxide nanoparticles do not penetrate the skin. Confocal laser scanning imaging has demonstrated that fluorescent polystyrene nanoparticles remain at the surface of the skin and appear to concentrate in and around hair follicles following a 2-hour exposure [12]. Multiphoton microscopy of fluorescently-labelled poly(lactide-co-glycolide) (PLGA) particles of ~300 nm diameter similarly showed that no penetration into/through the stratum corneum occurred [13].

However, dextran (1 μm) [14], iron (5 nm) [15], PLGA (1-10 μm) [16], quantum dots [17], and silver (25 nm) [18] particles have been reported to penetrate the skin barrier (although it is possible that the apparent permeation of silver may have occurred after dissolution of the particles). Even if the apparent, extensive penetration of certain nanoparticles (e.g., PLGA) may have been caused by accidental transfer during mechanical skin tissue sectioning, the issue remains controversial and requires resolution; there continue to be claims that nanoparticles included in pharmaceutical and cosmetic formulations, for example, are able to improve "active" penetration, at least partly due to the ability of the vectors to transport into and even through the skin [16,19,20]. The uncertainty is reflected in the concerns of the regulatory authorities charged with ensuring the safety of new products containing nanoparticles and, in particular, determining the potential risk of systemic exposure both across normal, intact skin and through skin, the barrier function of which may be compromised.

Confocal microscopy is an excellent technique for examining the internal, spatial disposition of fluorescent objects within the skin without need for physical sectioning. Since the skin does not require fixation or sectioning, artefacts associated with these techniques are prevented. Confocal microscopy, however, is unable to resolve individual nanoparticles; even with excellent optics, the diffraction limit for the resolution of green laser light is approximately 250 nm (hence, while individual particles of approximately 300 nm diameter have been discerned [13], smaller nanoparticles (≤ 100 nm) would not have been resolvable even with multiphoton imaging). Nevertheless, even though individual particles cannot be resolved, the fluorescence signal from these nano-structures far surpasses the skin's autofluorescence, which is not expected to change over the course of the experiments described here. Hence, any change in the pattern of the fluorescence signal must therefore be the result of translocation of the fluorophore.

In this paper, a quantitative approach is proposed and applied to the assessment of fluorescent nanoparticle disposition (i.e., spatial distribution) within the skin. Despite the fact that this method cannot reveal detailed mechanistic information, it is well-suited to address the basic question: "to what extent and depth are nanoparticles able to penetrate the skin's barrier?" The specific objective, therefore, was to undertake a quantitative analysis of the position of polymeric nanoparticles on the skin and to determine whether these structures penetrated the stratum corneum. The extent to which nanoparticle disposition was altered when stratum corneum integrity had been partially compromised was also considered.

MATERIALS AND METHODS

Materials

The skin disposition of Fluospheres® (Invitrogen Ltd, UK), which are covalently carboxy-modified, fluorescent, polystyrene particles with nominal diameters of 200, 100 and 20 nm, was assessed. Pig skin was obtained from a local abattoir, coarse hairs were trimmed and the tissue was dermatomed (Zimmer Electric Dermatome, Dover, Ohio, USA) to an approximate thickness of 750 μm. The skin was frozen and maintained at -20°C until required. Scotch book tape #845 (3M Media, Germany) was used to strip off the outer layers of the skin to induce minor damage to its barrier function. Skin surface lipids were removed from specified samples by washing with cold hexane (HPLC grade, Fisher Scientific Corporation, Loughborough, UK).

In vitro skin permeation

Prior to an experiment, the skin was thawed and any remaining hairs were carefully trimmed as close as possible to the surface. The tissue was clamped between the donor and the receptor compartments of a vertical Franz diffusion cell (area = 0.8 cm^2). The receptor compartment was carefully filled with warm phosphate-buffered saline (32°C, pH 7.4) allowing any bubbles to escape through the open port. A 100 μL aliquot of a 4.0 mg mL^{-1} aqueous suspension of Fluospheres®, or simply distilled water, was introduced into the donor chamber and sealed from the atmosphere using Parafilm®. The Franz cell was then placed in an oven at skin temperature (32°C) for the duration of the experiment. At the end of the exposure, the Franz cell was disassembled and excess surface liquid was gently absorbed with tissue. The centre of the sample was excised and placed on a slide for confocal microscopy. A drop of propylene glycol was placed on the sample immediately before imaging to minimize refractive index artefacts caused by potential air gaps under the coverslip.

At least four pieces of skin were exposed to aqueous suspensions of 200, 100 and 20 nm Fluospheres®, or to water alone. Samples were incubated for a range of times between 5 minutes and 16 hours. A control experiment involving application of a simple fluorescein solution in water was not performed, as the charged fluorophore does not penetrate into the skin to any measurable extent.

Subsequently, the experiments were repeated with skin, the barrier function of which had been partially compromised by removal of 4 tape-strips immediately prior to mounting in the Franz cell. Each tape was pressed firmly onto the skin sample and then removed in a single smooth movement. The direction of successive tape-strips was changed by 90° to improve the evenness of the process.

Sebum Removal

A skin sample was divided in two halves, one of which served as a control and was gently washed five times with 5 mL of water. The other piece was gently washed five times, with 5 mL of cold hexane (~4°C). Both samples were examined immediately post-washing using laser scanning confocal microscopy.

Laser scanning confocal microscopy

Images were obtained using a 510 Meta inverted confocal laser scanning microscope (Carl Zeiss, Jena, Germany). Samples were excited sequentially using 405 nm (diode), 488 nm (argon) and 633 nm (HeNe) lasers. A Plan-Apochromat 63×/1.40 oil DIC M27 objective was used for acquisition of all images. Fluorescence signals were recorded as three discrete channels at 420-480 nm (blue), 505-530 nm (green) and 647-754 nm (red), respectively.

Regions of interest were selected as coordinates from a 28×28 grid of 143×143 μm^2 fields of view using true random numbers generated using the internet-available resource: "Random.org" [21]. Each image stack recorded was 10-60 μm deep. Since the skin was not squashed flat by the coverslip, some fields of view selected showed a sloping skin surface across the image. The deeper stacks were recorded, therefore, to allow the entire image region to be analysed, without the need for subjective preference for flatter parts of the skin. Images in the z-direction were collected every micrometre. At least three random regions of interest were recorded for each skin sample. Randomly allocating these areas within the sample prevented selection bias of those offering the most attractive images. Furthermore, the entire image acquired was subjected to the analysis described below; i.e., all of the information collected was used to assess the behaviour under examination.

Image integration was performed at least twice for all samples to smooth noise from the photodiode detector. For the control samples, not treated with nanoparticles, the excitation intensity and gain were increased, and images were integrated at least four times to facilitate detection of autofluorescence and to smooth background noise.

Figure 1 shows five of the twenty *x*-*y* slices (at 0, 2, 4, 8 and 18 μm) from a typical *z*-stack, recorded from 0 to 19 μm through a region of interest. Areas, which are black, contained no measurable fluorescence. Red and blue areas represent autofluorescence from the skin, while green areas correspond to the presence of Fluospheres®. When combined, these images create a 3-dimensional fluorescence map of the sample as illustrated in **Supplementary Data 1**. Images were saved as 512×512 pixel.lsm files (a Zeiss proprietary format). Each file consisted of a hyperstack of three superimposed channels, where each channel comprised a stack of images of one colour recorded as a function of depth through the skin.

Subsequently, the red and blue channels of each image were merged and the resulting red/blue and green image stacks were converted to 128×128 pixel text image sequences using ImageJ [22]. Reducing the image size smoothes each pixel by a further 16-fold, thereby improving the signal-to-noise ratio at the cost of reducing the resolution.

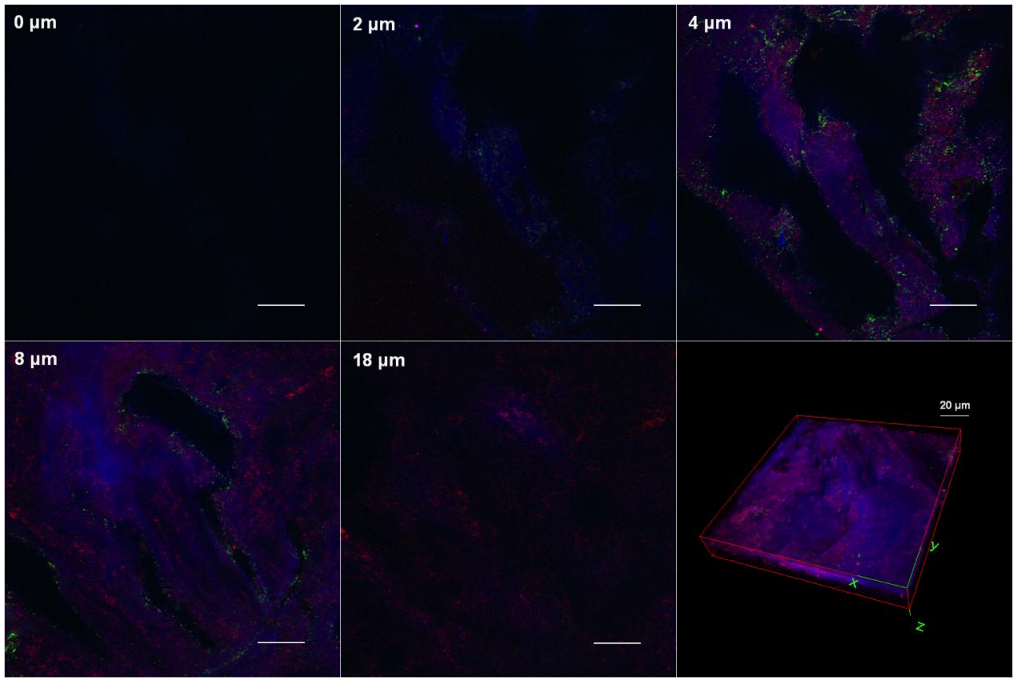

Figure 1: Fluorescence images of the distribution of 200 nm Fluospheres® on pig skin after a 16-hour exposure. Images were collected in the *x-y* plane from above the skin surface (0 µm) and then every 1 µm into the sample in the *z*-direction until green fluorescence was no longer visible. Five panels illustrate the results observed at different depths (2, 4, 8 and 18 µm) from the skin surface (0 µm). The last panel is a composite stack of all images recorded at each 1 µm step through the sample. The complete stack was rendered using the ImageJ 3D Viewer plugin. Scale bars are 20 µm. A 3-D reconstruction and animation of the stack is in *Supplementary Data 1*.

Image Analysis

The text images (i.e., data arrays containing the signal values for each pixel of each image) were analysed using the R statistical software package [23]. The autofluorescence signal (v) from the mixed red/blue channel can be examined to characterise the region corresponding to the skin within the image stack (as a function of depth, z). The edge of the skin was estimated using the midpoint parameter (T) of a sigmoid function [24].

$$v = B_A + \frac{A}{1+\exp(S)^{z-T}} \qquad (1)$$

where A is the amplitude, B_A is the background signal when no skin is present, and S is the sharpness of the edge. Note that the signal does not return to zero when an image is taken

outside the skin because of an offset in the minimal signal recorded. The majority of this signal is caused by extraneous scattered light striking the detector. The skin signal profile does not have a sharp edge since the volume that the microscope illuminates is finite; variations in the exact positions of the skin surface, varying concentrations of fluorescent compounds, and other sources of noise, cause smoothing of the profile. The fluorescence signal attenuates through the skin as the exciting and emitted beams are progressively absorbed and scattered with increasing path length.

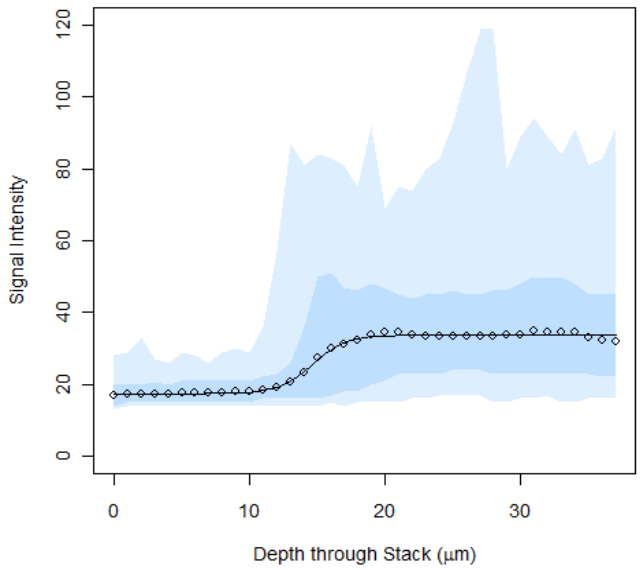

Figure 2: Sigmoid function (solid line) used to estimate location of the outer skin edge through a 36×36 μm² quadrant from a typical region of interest. The data points represent the mean values, the light blue area shows the range of the data, while the darker blue region indicates the first to ninth deciles.

Figure 2 illustrates how the autofluorescence signal varies in a sampling region with depth through the *z*-stack. For many images, this function can be used to estimate the outer edge of the skin. However, the sigmoid function was not robust for images where the signal decayed below the surface of the skin. In these cases, the edge was found by truncating the image to exclude the deeper skin where the signal had begun to fall off. Any missing values were estimated by comparing the successfully calculated values from Equation (1) with the position of the autofluorescence signal (v) maximum near the skin surface. The position in the image stack (z) of the outer edge of the skin was estimated using Equation (2):

$$v = F_A \cdot \frac{\exp\left\{-\left(z - M_A\right)^2 / 2W_A{}^2\right\}}{W_A\sqrt{2\pi}} \qquad (2)$$

which describes a normal distribution where F_A is an area parameter, M_A is the midpoint parameter (determined at the peak of the autofluorescence signal), and W_A is the peak width parameter.

The position of the edge, T, was then subtracted from the distance (z) through the image to calculate the depth (d) into the skin of the green channel signal intensity (u) in each of sixteen 36×36 μm² quadrants. Sources of error in this approach include uncertainty in the precise location of the skin surface, variability in the brightness of the autofluorescence signal, and differences in the disposition of particles across each skin sample. The distribution of particles was defined within a bounded region of the skin. The profile of the green channel signal across the skin was deduced by inspection to be log-normal, and conformed, therefore, to the relationship:

$$f(d) = \frac{\exp\left\{-\left(\log(d) - M_S\right)^2 / 2W_S{}^2\right\}}{d \cdot W_S \sqrt{2\pi}} \tag{3}$$

where M_S and W_S are the mean and standard deviation (in log units) of the log-normal distribution [25]. So that the distribution could be fitted directly to the data, the signal intensity was modelled using two additional parameters such that:

$$u = B_S + F_S \cdot f(d) \tag{4}$$

where B_S represents a background correction factor and F_S is an expansion factor.

Figure 3 shows the sum of the green fluorescence signals (u) in each quadrant of a region of interest through the sample (d). The median position of a log-normal distribution is the exponential of the peak position, M_S. The latter was calculated from the parameters of the fit for each quadrant. To determine whether the Fluospheres® moved into the skin with increasing duration of contact, these median peak positions were compared over time. For some images, the signal-to-noise ratio of the fluorescence was too low to determine the profile. Also, occasionally, when the skin surface in the region of interest was very uneven, the model was not always able to converge on a solution.

For each randomly chosen area on each skin sample, a profile of the green signal distribution was generated with very few human decisions required, thereby reducing the subjectivity inherent in image interpretation and improving reliability. In this way, the derived parameters describing the profiles can be compared across images to assess whether the nanoparticles, which are too small to resolve optically, were actually penetrating beyond the skin surface or not. Emphasis should not be placed on the absolute signal intensities, as the gain was adjusted to maximise the dynamic range of data collection from each image. No pixels recorded a signal

of zero, and the lowest values were typically ~20 (**Figure 2**). Each quadrant contained 1024 pixels and, since each image was recorded at a fixed scale, background subtraction and normalization were not required. The parameters shown on Equation (4) were used instead, with $B_S \approx 14000$. Because the total signal from each image is the sum of autofluorescence and that from the Fluospheres, and as both signals can vary between images, the absolute signal intensities cannot be reliably interpreted. However, signal distribution would vary if there were penetration of nanoparticles. Hence, when using the log-normal distribution as described, the position of peak fluorescence is the best description of particle penetration.

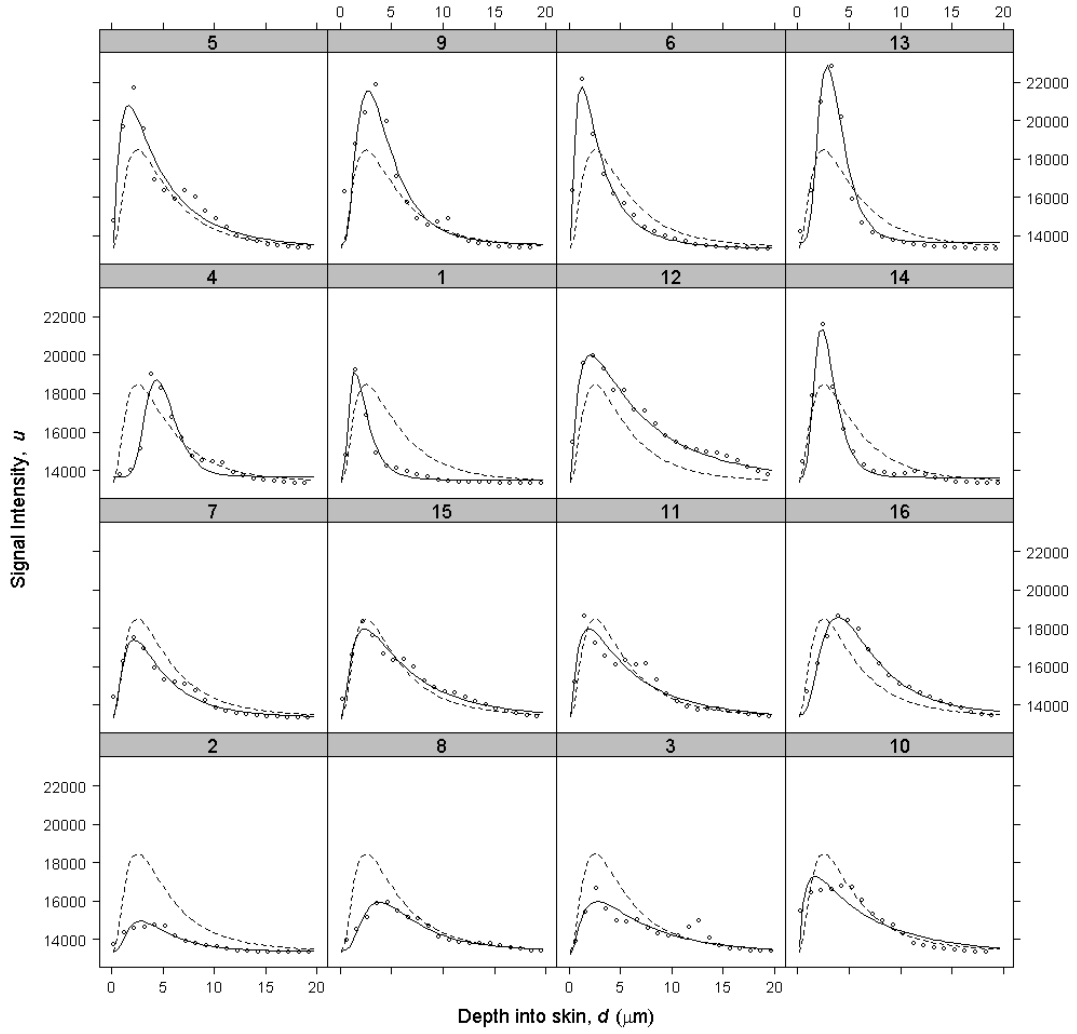

Figure 3: Distribution of green signal intensity (u) in one 143×143 μm² region of skin following application of 200 nm Fluospheres® for 16 hr. A log-normal distribution (Equation (3)) was fitted to the data for each of sixteen 36×36 μm² quadrants using non-linear mixed effects modelling with R software. Dashed lines show the population mean profile; solid lines show the local mean for each quadrant.

RESULTS AND DISCUSSION

The blue fluorescent layer observed at the surface of untreated (control) pig skin corresponds to excitation with the diode laser at 405 nm (**Figure 4, panels a-d**). The most likely origin of this signal is sebum which has been shown to fluoresce when excited with UV light [26]. Confirmation of this idea is reflected in the variable intensity of the blue fluorescence seen in the images obtained and, in particular, by the maxima found in the region of hair follicles, via which sebum is secreted from the pilosebaceous glands (see **TOC graphic** for an example).

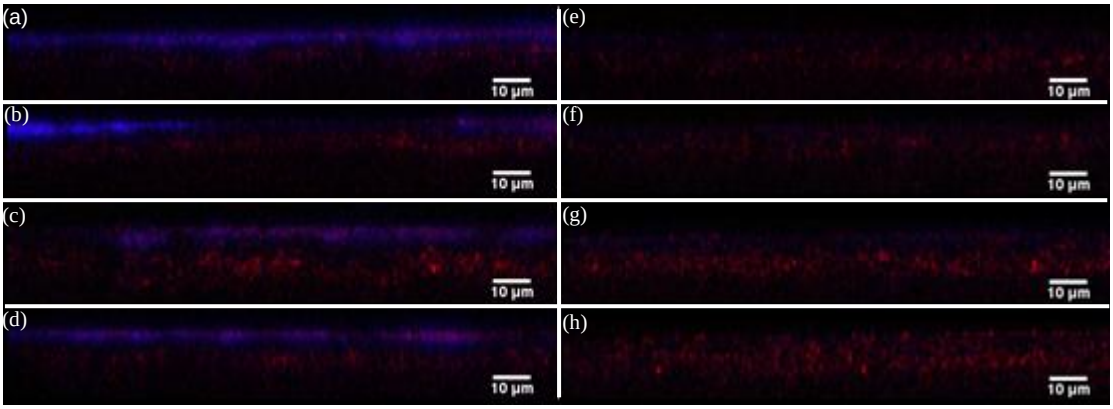

Figure 4: Cross-sections through four pieces of pig skin derived from confocal microscopy stacks of serial x-y images. Each skin piece was divided in half and examined either "as is" (panels a-d) or post-washing with cold hexane (panels e-h). The dotted line indicates the approximate position of the skin surface.

Sebum is composed of a mixture of lipids (triglycerides, wax esters, squalene and small amounts of cholesterol esters). When it emerges onto the skin surface, it mixes with the lipids of the stratum corneum to form a superficial lipid film [27]. Washing skin with cold hexane has been shown to remove skin surface lipids without affecting skin barrier function i.e. without altering transepidermal water loss [28]. This treatment decreased considerably the intensity of the blue fluorescent layer compared to the control (**Figure 4, panels e-h**); in some cases, post-washing with hexane, only the red autofluorescence from deeper skin layers remained. The results are fully consistent with an earlier investigation using infrared spectroscopy, which revealed a significant presence of sebaceous lipids in the outer layers of human stratum corneum *in vivo* [29].

Fluospheres® were visible in the top layers of the stratum corneum after a short 5 minute contact with intact skin. However, no further penetration appeared to take place over the next 16 h. **Figure 5** shows typical cross-sections through the skin as converted from confocal microscopy stacks of serial x-y images. Although the laser power and gain were increased for blank samples, the intensity of the green signal was rather low compared to images of

Fluospheres®. Random speckle throughout the green channel indicates where the gain had been increased due to a lack of strongly fluorescing regions. **Supplementary data 2, 3, and 4** contain animated scans (from which the images in **Figure 5** were extracted) across the skin samples examined post-treatment with the fluorescent nanoparticles of different diameters, while **Supplementary data 5** presents the control, untreated results. The fluorescence densities from the different size nanoparticles were similar from sample to sample and were not correlated with the calculated fluorescein equivalents per nanoparticle volume (which varied by about 3-fold between the different particle diameters employed). In any case, as the objective of the experiments was to examine fluorescence *distribution*, rather than absolute intensity, it was not necessary to control precisely the total fluorescence applied to the skin.

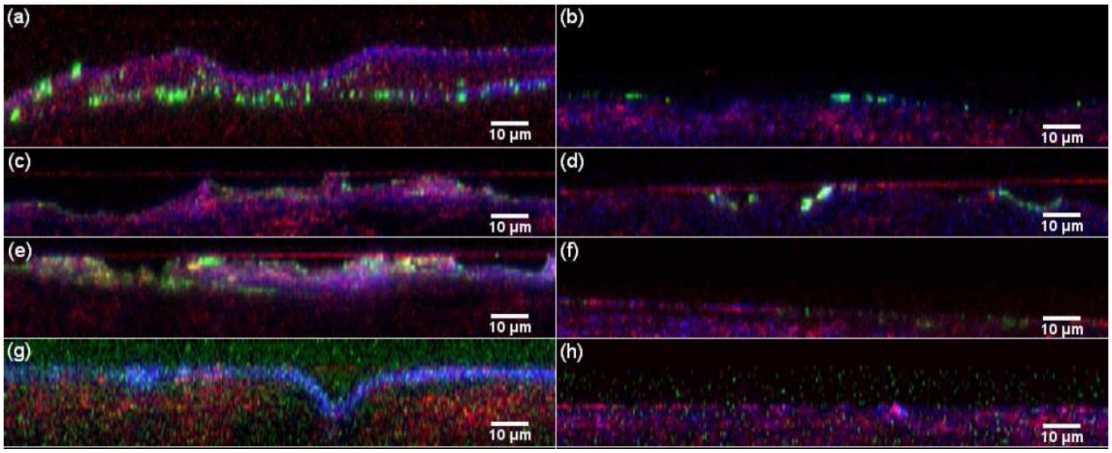

Figure 5: Confocal microscopy cross-sections of the upper layers of pig skin following a 5-minute application of 200 nm (a,b), 100 nm (c,d), and 20 nm Fluospheres® (e,f), and water (g,h). Panels a, c, e and g are images post-administration to intact skin, whereas panels b, d, f and h show representative results following delivery to tape-stripped skin. The horizontal red line in some images was caused by reflection from the coverslip interface when the channel gain was increased. See also *Supplementary data 2-5.*

Figure 6 shows the estimated depth of the green fluorescent signal peak in the stratum corneum after exposure of the skin to Fluospheres® of different diameters or to water alone (the 'blank' experiments). The duration of contact between the formulations and the skin did not alter the results in any perceptible fashion. No particle aggregation was observed in the suspensions prior to their application to the skin, although the possibility that aggregation may have occurred once the nanoparticles made contact with the skin surface cannot be ruled out. The fact that particles were observed at apparent depths of 2-3 µm probably corresponds to their infiltration into/through the stratum disjunctum, the most superficial layer of the stratum corneum consisting of loosely associated and desquamating corneocytes [30]. The similar

disposition seen in tape-stripped skin may reflect a small mechanical perturbation of the barrier provoked by removal of the adhesive.

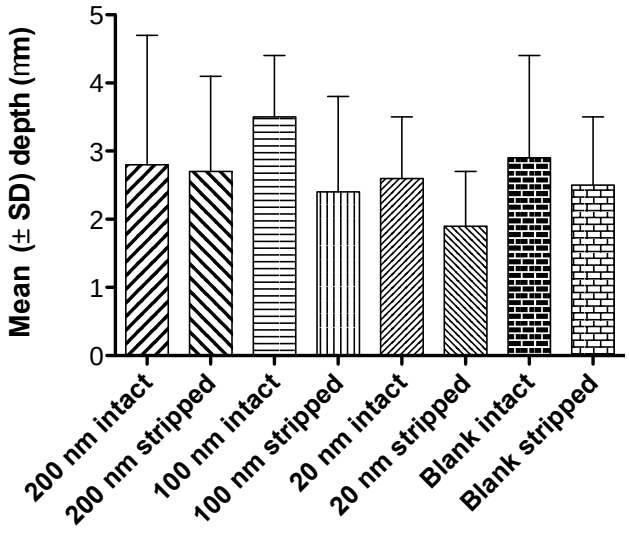

<u>Figure 6</u>: Position of peak fluorescence/autofluorescence for particles and blank samples. Error bars show standard deviation. There were no differences between samples observed at different exposure times. Peak signal was observed at a greater depth in intact skin than in stripped skin.

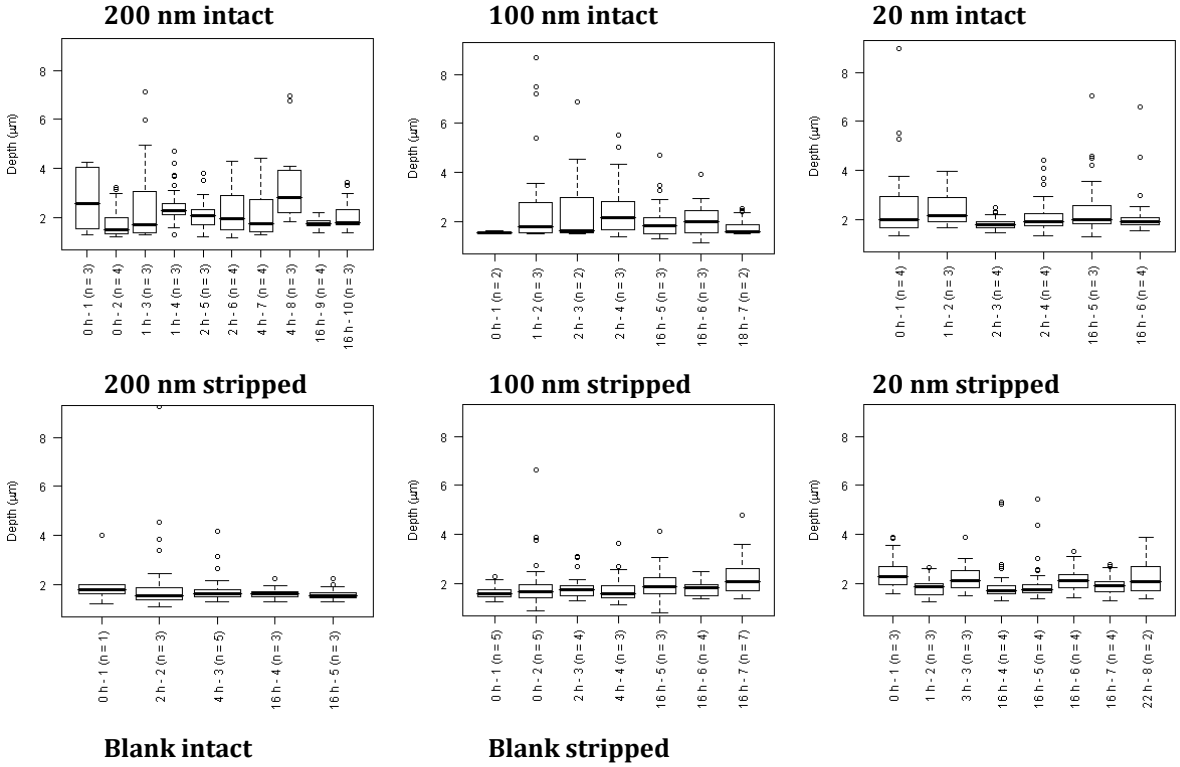

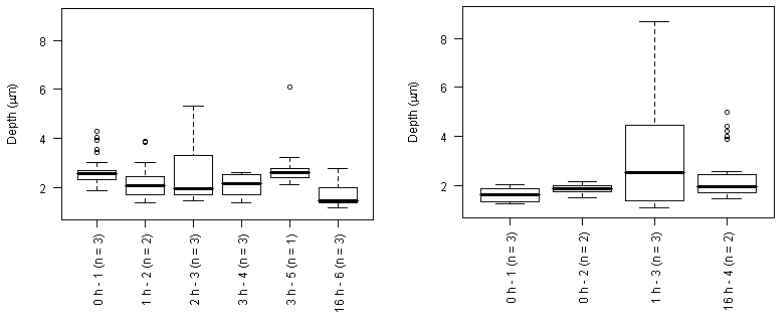

Figure 7: Spatial distribution of fluorescent nanoparticles of different diameters as a function of time of exposure to the skin (both intact and tape-stripped – upper six panels). The lower two panels show the distribution of skin autofluorescence in intact and tape-stripped samples.

These conclusions are reinforced by the data in **Figure 7**, which illustrates the evolution over time of the spatial distributions of the 200, 100 and 20 nm fluorescent particles within the stratum corneum of intact and tape-stripped skin. The figure also shows that the pattern of green autofluorescence from untreated (intact and tape-stripped) skin does not change with time, confirming that there is no significant redistribution of the faintly fluorescent endogenous species during the experiment.

Figure 7 demonstrates clearly that there was no time-dependent penetration of any of the Fluospheres® examined. The apparent distribution profile of the particles appears from the boxplots to be slightly wider in intact skin than in tape-stripped skin. As suggested above, this would be consistent with particles infiltrating with little resistance into and through the desquamating layer of the stratum corneum (see the left-hand panels in **Figure 5**). This hypothesis is supported by the fact that this disposition occurs within the first 5 minutes of skin contact but that, thereafter, negligible change in the profile occurs over the next 16 hours (and further evidence may be visualised clearly in the animated scans in **Supplementary data 2-5**).

It should be emphasised that this research has clearly not been able to make a systematic evaluation of nanoparticle disposition on the skin for the entire spectrum of particle properties, including shape and charge (although some results with respect to the latter parameter have been reported [31]). The impact of such other important variables remains to be determined. Further, while the conclusions to be drawn from the data presented here are somewhat unequivocal, the observations and their analysis cannot explain, with any degree of certainty, why others have reported nanoparticle uptake into living skin layers following their topical application (e.g., [15,17]). While speculative alternatives might be proposed, such as accidental contamination on sectioning, or invisible flaws in skin integrity (across which, for example, a very small quantum dot of a few nanometres diameter might be able to travel), complete understanding will only be possible with further, scrupulously controlled experiments coupled with objective data analysis and interpretation. Finally, although a number of previous

publications have pointed out the sequestration of nanoparticles in and around follicular structures [11,12,32], this behaviour (which can be observed in the animated scan in **Supplementary data 4**, for example) has been overly emphasised here because of the reported contraction of follicles that occurs when mammalian skin is dermatomed [33].

Thus, the method described in this paper represents an objective evaluation of nanoparticle disposition post-application to the skin. The strategy used takes into consideration the potentially confounding effects of autofluorescence, and the statistical approach to data analysis reduces substantially the uncertainty associated with sample-to-sample variability, random imperfections in skin barrier function (resulting, for example, from tissue handling), fluctuations in laser performance, etc. Confocal imaging, which avoids mechanical sectioning of the tissue under examination, also allows the impact of a convoluted skin surface (that might give rise to an apparent "deep" penetration of particles as they are deposited into a fold or an invagination of the sample) to be visualised unambiguously and interpreted accordingly. The quantitative findings reported here support the more qualitative imaging data that has been previously described [12, 29], and which points persuasively to the efficient manner in which the stratum corneum excludes the ingress of particulate nanomaterials beyond the most superficial part of the barrier.

CONCLUSIONS

Polymeric nanoparticles (ranging in diameter from 20 to 200 nm) were observed to penetrate only into the surface layers (approximate depth of 2-3 μm) of the stratum corneum. This is interpreted as infiltration along fissures in the stratum disjunctum. Using quantitative analysis of bulk particle location, no time-dependent penetration of nanoparticles was observed, even when the barrier was partially compromised by adhesive tape-stripping. It follows that such particles, when appropriately formulated, may prove useful as drug reservoirs which remain on or near to the skin surface and from which controlled release may be sustained over extended periods of time.

ACKNOWLEDGEMENTS

Supported by the European Commission 6th Research and Technological Development Framework Programme (NAPOLEON: NAnostructured waterborne POLymEr films with OutstaNding properties). L.R.C.-R. is the recipient of a doctoral fellowship from CONACyT, Mexico.

FIGURE LEGENDS

Figure 1: Fluorescence images of the distribution of 200 nm Fluospheres® on pig skin after a 16-hour exposure. Images were collected in the *x-y* plane from above the skin surface (0 μm) and then every 1 μm into the sample in the *z*-direction until green fluorescence was no longer visible. Five panels illustrate the results observed at different depths (2, 4, 8 and 18 μm) from the skin surface (0 μm). The last panel is a composite stack of all images recorded at each 1 μm step through the sample. The complete stack was rendered using the ImageJ 3D Viewer plugin. Scale bars are 20 μm. A 3-D reconstruction and animation of the stack is in *Supplementary Data 1*.

Figure 2: Sigmoid function (solid line) used to estimate location of the outer skin edge through a 36×36 μm^2 quadrant from a typical region of interest. The data points represent the mean values, the light blue area shows the range of the data, while the darker blue region indicates the first to ninth deciles.

Figure 3: Distribution of green signal intensity (u) in one 143×143 μm^2 region of skin following application of 200 nm Fluospheres® for 16 hr. A log-normal distribution (Equation (3)) was fitted to the data for each of sixteen 36×36 μm^2 quadrants using non-linear mixed effects modelling with R software. Dashed lines show the population mean profile; solid lines show the local mean for each quadrant.

Figure 4: Cross-sections through four pieces of pig skin derived from confocal microscopy stacks of serial x-y images. Each skin piece was divided in half and examined either "as is" (panels a-d) or post-washing with cold hexane (panels e-h). The dotted line indicates the approximate position of the skin surface.

Figure 5: Confocal microscopy cross-sections of the upper layers of pig skin following a 5-minute application of 200 nm (a,b), 100 nm (c,d), and 20 nm Fluospheres® (e,f), and water (g,h). Panels a, c, e and g are images post-administration to intact skin, whereas panels b, d, f and h show representative results following delivery to tape-stripped skin. The horizontal red line in some images was caused by reflection from the coverslip interface when the channel gain was increased. See also *Supplementary data 2-5.*

Figure 6: Position of peak fluorescence/autofluorescence for particles and blank samples. Error bars show standard deviation. There were no differences between samples observed at different exposure times. Peak signal was observed at a greater depth in intact skin than in stripped skin.

Figure 7: Spatial distribution of fluorescent nanoparticles of different diameters as a function of time of exposure to the skin (both intact and tape-stripped – upper six panels). The lower two panels show the distribution of skin autofluorescence in intact and tape-stripped samples.

SUPPLEMENTARY FILES

1. A 3-D reconstruction and animation of the composite stack of all images in the final (bottom right-hand) panel of Figure 1.
2. Animated scan (from which the images in panels a and b of **Figure 5** were extracted) across the skin samples examined post-treatment with 200 nm diameter fluorescent nanoparticles. of different diameters, while **Supplementary data 5** presents the control, untreated results.
3. Animated scan (from which the images in panels c and d of **Figure 5** were extracted) across the skin samples examined post-treatment with 100 nm diameter fluorescent nanoparticles.
4. Animated scan (from which the images in panels e and f of **Figure 5** were extracted) across the skin samples examined post-treatment with 20 nm diameter fluorescent nanoparticles.
5. Animated scan (from which the images in panels g and h of **Figure 5** were extracted) across the skin samples examined post-treatment with water alone (i.e., the control).

REFERENCES

[1] P.H. Hoet, I. Bruske-Hohlfeld, O.V. Salata, Nanoparticles - known and unknown health risks, J. Nanobiotechnology 2 (2004) 12.

[2] D.M. Brown, K. Donaldson, P.J. Borm, R.P. Schins, M. Dehnhardt, P. Gilmour, L.A. Jimenez, V. Stone, Calcium and ROS-mediated activation of transcription factors and TNF-alpha cytokine gene expression in macrophages exposed to ultrafine particles Am. J. Physiol. Lung Cell Mol. Physiol., 286 (2004) L344-353.

[3] K.O. Yu, C.M. Grabinski, A.M. Schrand, R.C. Murdock, W. Wang, B. Gu, et al., Toxicity of amorphous silica nanoparticles in mouse keratinocytes, J Nanopart. Res. 11 (2009) 15-24.

[4] D. Papakostas, F. Rancan, W. Sterry, U. Blume-Peytavi, A. Vogt, Nanoparticles in dermatology, Arch. Dermatol. Res. 303 (2011) 533-550.

[5] R.H. Neubert. Potentials of new nanocarriers for dermal and transdermal drug delivery, Eur. J. Pharm. Biopharm. 77 (2011) 1-2.

[6] K.C. Madison, Barrier function of the skin: “la raison d'Être” of the epidermis, J. Invest. Dermatol. 121 (2003) 231-241.

[7] M.J. Cork, S.G. Danby, Y. Vasilopoulos, J. Hadgraft, M.E. Lane, M. Moustafa, R.H.Guy, A.L. Macgowan, R.Tazi-Ahnini, S.J. Ward, Epidermal barrier dysfunction in atopic dermatitis, J. Invest. Dermatol. 129 (2009) 1892-1908.

[8] A.S Dussert, E. Gooris, J. Hemmerle, Characterization of the mineral content of a physical sunscreen emulsion and its distribution onto human stratum corneum, Int. J. Cosmetic Sci. 19 (1997) 119-129.

[9] S.E. Cross, B. Innes, M.S. Roberts, T. Tsuzuki, T.A. Robertson, P. McCormick, Human skin penetration of sunscreen nanoparticles: in-vitro assessment of a novel micronized zinc oxide formulation, Skin Pharmacol. Physiol. 20 (2007) 148-154.

[10] A.O. Gamer, E. Leibold, B. van Ravenzwaay, The in vitro absorption of microfine zinc oxide and titanium dioxide through porcine skin, Toxicol. In Vitro 20 (2006) 301-307.

[11] J. Lademann, H. Weigmann, C. Rickmeyer, H. Barthelmes, H. Schaefer, G. Mueller, W. Sterry, Penetration of titanium dioxide microparticles in a sunscreen formulation into the horny layer and the follicular orifice, Skin Pharmacol. Appl. Skin Physiol. 12 (1999) 247-256.

[12] R. Alvarez-Roman, A. Naik, Y.N. Kalia, R.H. Guy, H. Fessi, Skin penetration and distribution of polymeric nanoparticles, J Controlled Release 99 (2004): 53-62.

[13] F. Stracke, B. Weiss, C.-M. Lehr, K.König, U.F. Schaefer, M. Scheider, Multiphoton microscopy for the investigation of dermal penetration of nanoparticle-borne drugs, J Invest Dermatol 126 (2006) 2224-2233.

[14] S.S. Tinkle, J.M Antonini, B.A. Rich, J.R Roberts, R. Salmen, K. DePree, E.J. Adkins, Skin as a route of exposure and sensitization in chronic beryllium disease, Environ. Health Perspect. 111 (2003) 1202-1208.

[15] B. Baroli , M.G. Ennas, F. Loffredo, M. Isola, R. Pinna, M.A. Lopez-Quintela, Penetration of metallic nanoparticles in human full-thickness skin, J. Invest. Dermatol. 127 (2007) 1701-1712.

[16] E.G. de Jalon, M.J. Blanco-Prieto, P. Ygartua, S. Santoyo, G. Maina, PLGA microparticles: possible vehicles for topical drug delivery, Int. J. Pharm. 226 (2001) 181-184.

[17] T.W. Prow, N.A. Monteiro-Riviere, A.O. Inman, J.E. Grice, X. Chen, X. Zhao, W.H. Sanchez, A. Gierden, M.A. Kendall, A.V. Zvyagin, D. Erdmann, J.E. Riviere, M.S. Roberts, Quantum dot penetration into viable human skin, Nanotoxicology 6 (2012) 173-185.

[18] F.F. Larese, F. D'Agostin, M. Crosera, G. Adami, N. Renzi, M. Bovenzi M, et al., Human skin penetration of silver nanoparticles through intact and damaged skin, Toxicology 255 (2009) 33-37.

[19] S. Miyazaki, A. Takahashi, W. Kubo, J. Bachynsky, R. Loebenberg, Poly n-butylcyanoacrylate (PNBCA) nanocapsules as a carrier for NSAIDs: in vitro release and in vivo skin penetration, J. Pharm. Pharm. Sci. 6 (2003) 238-245.

[20] J. Wu, W. Liu, C. Xue, S. Zhou, F. Lan, L. Bi, H. Xu, X. Yang, F.D. Zeng, Toxicity and penetration of TiO_2 nanoparticles in hairless mice and porcine skin after subchronic dermal exposure, Toxicol. Lett. 191 (2009) 1-8.

[21] Random.org. Dublin, Ireland: Haahr M; 1998-2012 [updated 12 February 2012; cited 2012]. Available from: www.random.org.

[22] M. Abramoff, P. Magalhães, S. Ram, Image processing with ImageJ, Biophotonics Int. 11 (2004) 36-42.

[23] R Development Core Team. R: A language and environment for statistical computing. Vienna, Austria: R Foundation for Statistical Computing; 2007.

[24] C. Ela, O. Ahmet, Modelling of edge profiles in pigmented skin lesions In: Houston A, Zwiggelaar R, editors. Medical Image Understanding and Analysis. BMVA Press; Portsmouth. (2002) 3-6.

[25] J. Aitchison, J.A.C. Brown. The Log-normal Distribution. Cambridge University Press. 1957.

[26] S.W. Youn, J.H. Kim, J.E. Lee, S.O. Kim, K.C. Park, The facial red fluorescence of ultraviolet photography: is this color due to Propionibacterium acnes or the unknown content of secreted sebum? Skin Res. Technol. 15 (2009) 230-236.

[27] H.M. Sheu, S.C. Chao, T.W. Wong, J. Yu-Yun Lee, J.C. Tsai, Human skin surface lipid film: an ultrastructural study and interaction with corneocytes and intercellular lipid lamellae of the stratum corneum, Br. J. Dermatol. 140 (1999) 385-391.

[28] K. Abrams, J.D. Harvell, D. Shriner, P. Wertz, H. Maibach, H.I. Maibach, S.J. Rehfeld, Effect of organic solvents on in vitro human skin water barrier function, J. Invest. Dermatol. 101 (1993) 609-613.

[29] D. Bommannan, R.O. Potts, R.H. Guy, Examination of stratum corneum barrier function in vivo by infrared spectroscopy, J. Invest. Dermatol. 95 (1990) 403-408.

[30] M. Simon, N. Jonca, M. Guerrin, M. Haftek, D. Bernard, C. Caubet, T. Egelrud, R. Schmidt, G. Serre, Refined characterization of corneodesmosin proteolysis during terminal differentiation of human epidermis and its relationship to desquamation, J. Biol. Chem. 276 (2001) 20292-20299.

[31] X. Wu, K. Landfester, A. Musyanovych, R.H. Guy, Disposition of charged nanoparticles after their topical application to the skin, Skin Pharmacol Physiol. 23 (2010) 117-23.

[32] X. Wu, G.J. Price, R.H. Guy, Disposition of nanoparticles and an associated lipophilic permeant following topical application to the skin, Mol. Pharmaceutics 6 (2009) 1441-1448.

[33] A. Patzelt, H. Richter, R. Buettemeyer, H. J. Roewert Huber, U. Blume-Peytavi, W. Sterry, J. Lademann, Differential stripping demonstrates a significant reduction of the hair follicle reservoir in vitro compared to in vivo, Eur J Pharm Biopharm 70 (2008) 234-238.